Biochemistry and Biophysics Reports 42 (2025) 102006

Contents lists available at ScienceDirect

Biochemistry and Biophysics Reports

journal homepage: www.elsevier.com/locate/bbrep

# Fibroblasts fluctuating between mesenchyme and epithelium are involved in hair follicle mesenchyme development

Yoshikazu Hirose [a], Asaka Miura [a], Yuya Ouchi [a,b], Tomomi Kitayama [a,b], Souki Omura [c], Takashi Shimbo [a,d], Akio Tanaka [e], Manabu Fujimoto [f], Kotaro Saga [a], Katsuto Tamai [a,b,*]

[a] Department of Stem Cell Therapy Science, Graduate School of Medicine, Osaka University, Suita, Osaka, Japan
[b] StemRIM Inc., Ibaraki, Osaka, Japan
[c] School of Medicine, Hiroshima University, Hiroshima, Japan
[d] StemRIM Institute of Regeneration-Inducing Medicine, Osaka University, Suita, Osaka, Japan
[e] Department of Dermatology, Graduate School of Biomedical and Health Sciences, Hiroshima University, Hiroshima, Japan
[f] Department of Dermatology, Graduate School of Medicine, Osaka University, Suita, Osaka, Japan

ARTICLE INFO

*Keywords:*
EMT/MET
Skin development
Hair follicle dermal stem cell
Single-cell RNA sequencing

ABSTRACT

The transition between the mesenchyme and epithelium contributes to the development of various tissues. During skin development, epithelial-mesenchymal transition in the ectodermal epithelia is involved in the development of the dermal mesenchyme in early embryos. However, the precise roles and functions of epithelial-mesenchymal/mesenchymal-epithelial transition in cutaneous development have not been fully elucidated. In this study, we aimed to elucidate these roles and functions in the neonatal mouse skin. We conducted single-cell RNA sequencing and immunohistochemical analyses to search for *Pdgfra*-expressing ($P\alpha^+$) fibroblasts with transition activities to/from *Krt5*-expressing keratinocytes. We determined that the $P\alpha^+$/*Krt5*-lineage ($K5^{lin+}$) fibroblasts significantly contributed to developing hair follicle dermal stem cells to generate lower dermal papilla cells and lower dermal sheath cells. In the developing mouse skin, $K5^{lin+}$ fibroblasts appeared concurrently with hair follicle development and formed outer edge cells in the early dermal papilla on embryonic day 16.5. $K5^{lin+}$ hair follicle mesenchymal cells were also maintained in aged mouse skin. These results provide insights into the role and function of the transition between the mesenchyme and epithelium in hair follicle development and maintenance.

## 1. Introduction

Transitions between epithelia and mesenchyme (EMT) and vice versa (MET) are critical biological mechanisms for the development and regeneration of cutaneous tissues. During the regenerative process, EMT occurs at the edge of the epidermal wound to re-distribute epidermal stem/progenitor cells by transitioning them to migrating mesenchymal cells on the wound bed [1]. In early embryos, EMT in the single-layer ectoderm epithelium at the neural fold and neural tube forms the ectomesenchyme/neural crest, which then generates fibroblasts [2], dermal papilla cells (DPCs) [3], melanocytes, Schwann cells, and peripheral nerve cells [4] in the skin. Facial and head dermal fibroblasts derived from the neural crest are representative fibroblasts generated by EMT during development, and murine vibrissal papillae are neural-crest-derived cells [5]. In addition, the dermal papillae of fetuses and adults temporally express Snai1 and Snai2, which are involved in EMT, implying the EMT supplies mesenchymal cells to hair follicles, where epidermal cells and mesenchymal cells are closely linked [6,7]. These findings illustrate the contribution of the dynamic transition between the mesenchyme and epithelia in the development and maintenance of cutaneous structures and functions, particularly in dermal papillae. However, the existence and characteristics of fibroblasts that show the lineage of epidermal cell markers in dermis, including the dermal papilla, remain unclear.

In this study, through single-cell RNA sequencing (scRNA-seq) and immunohistochemistry, we investigated the transition between platelet-derived growth factor alpha (*Pdgfra*)-expressing ($P\alpha^+$) mesenchymal cells and keratin 5 (*Krt5*)-expressing epithelial cells in the developing neonatal and fetal skin of mice. Our primary aim was to elucidate the characters of mesenchymal cells which showed the epithelial cell

* Corresponding author. Osaka University Graduate School of Medicine, 2-2, Yamadaoka, Suita, Osaka, 565-0871, Japan.
*E-mail address:* tamai@sts.med.osaka-u.ac.jp (K. Tamai).

https://doi.org/10.1016/j.bbrep.2025.102006
Received 15 January 2025; Received in revised form 24 March 2025; Accepted 3 April 2025

lineage during cutaneous development. We identified the contribution of the *Krt5*-lineage+ (*K5*$^{lin+}$) fibroblasts to the development of hair follicle dermal stem cells (hfDSCs).

## 2. Results

### 2.1. Transcriptomic identification of *K5*$^{l+}$ fibroblasts in the follicular mesenchyme

To identify *Pα*$^{+}$ fibroblast populations transitioning from/to *Krt5*$^{+}$ epithelial cells, we used *Pdgfra*-H2B-EGFP;*Krt5*-Cre; ROSA-CAG-loxP-stop-loxP-tdTomato (*Pα*-EGFP/*K5*$^{lin}$-tdTomato) mice, in which *Pα*$^{+}$/*K5*$^{lin+}$ fibroblasts could be traced using eGFP/tdTomato fluorescence. Full-thickness skin was harvested from the head, back, and abdomen of the three neonatal mice, and obtained cell suspensions were pooled, then the *K5*$^{lin+}$ and *K5*$^{lin−}$ fibroblasts were FACS-sorted as eGFP$^{+}$/tdTomato$^{+}$ and eGFP$^{+}$/tdTomato$^{−}$ cells, respectively (Fig. 1a, Supplementary Fig. 1). We identified *K5*$^{lin+}$ fibroblasts, which accounted for 2.4 % of the total skin cells and 4.7 % within the total fibroblasts (Fig. 1b).

We then subjected the FACS-sorted *K5*$^{lin+}$ and *K5*$^{lin−}$ fibroblasts to scRNA-seq analyses. Unsupervised clustering of fibroblasts identified 10 clusters, including arrector pili muscle cells and adipocytes (Fig. 1c and d). As Fig. 1e shows, the proportion of *K5*$^{lin+}$ fibroblasts of the whole fibroblasts were relatively higher in Fib1 (1.70 %) and Fib7 (1.23 %) clusters than in other clusters (up to 0.5 %), such as Fib3 (0.14 %). The Fib1 cluster was characterized as DPCs by gene signatures, including *Alx4* and *Prom1*, and the Fib7 cluster dominated only in the head skin based on genes specific to the deep dermis, such as *Dlk1* and *Mgp* (Fig. 1f), while the Fib3 cluster was identified as superficial dermal fibroblasts expressing *Dpp4* and *Lrig1*. These results highlighted that *K5*$^{lin+}$ fibroblasts uniquely form a part of dermal papilla and deep dermis. Subsequently, we focused on Fib1 cluster, as *K5*$^{lin+}$ fibroblasts were distributed to the whole body. To analyze differences between *K5*$^{lin+}$ and *K5*$^{lin−}$ fibroblasts in the Fib1 cluster, we analyzed the differential expression of genes between them in the Fib1 cluster of the dorsal skin. We found that the *K5*$^{lin+}$ fibroblasts predominantly expressed *Col11a1*, *Acta2*, and *Tagln* genes, as well as *Ednrb* and *Cd200*, which are specifically expressed in dermal sheath cells (DSCs) (Fig. 1g and h, Supplementary Table 1), suggesting a preferential contribution of *K5*$^{lin+}$ fibroblasts to the follicular mesenchyme, such as DPCs and DSCs. *K5*$^{lin+}$ fibroblasts dominantly expressed smooth muscle-related genes, such as *Acta2*, *Tagln*, and *Tpm1*, which was consistent with the contractile characteristics of DSCs, while upregulated genes of *K5*$^{lin−}$ fibroblasts were involved in the BMP signaling pathway (Bmp3, Bmp4, and Bmp7), which is essential for hair follicle generation and maintenance of epithelial progenitors [8,9]. Additionally, *K5*$^{lin+}$ fibroblasts shared approximately 50 % of the fibroblasts expressing both *Sox2* and *Acta2*, representative marker genes for hfDSCs, which are the exclusive population of DSCs showing multipotency [10] (Fig. 1h).

### 2.2. Histological distribution of *K5*$^{lin+}$ fibroblasts in lower dermal papilla and lower dermal sheath

To explore the localization of *K5*$^{lin+}$ fibroblasts in the skin, we histologically analyzed the dorsal skin of *Pα*-EGFP/*K5*$^{lin}$-tdTomato neonatal mice. As shown in the scRNA-seq analyses, eGFP and tdTomato double-positive *K5*$^{lin+}$ fibroblasts were observed in the DPCs and DSCs of hair follicles, which were characterized by the expression of SOX2 and CD200 proteins, respectively (Fig. 2a). The *K5*$^{lin+}$ fibroblasts were also located at the lowest edge of hair follicles (dermal sheath cup) and were characterized by the expression of both SOX2 and αSMA, consistent with the hfDSCs providing lower DPCs and DSCs. Notably, none of the *K5*$^{lin+}$ cells expressed KRT5 protein, confirming that they were indeed fibroblasts and not keratinocytes. To evaluate the proportion of *K5*$^{lin+}$ fibroblasts in the dermal papilla, randomly selected 45 hair follicles in the dorsal skin of three neonatal mice were analyzed. The percentage of *K5*$^{lin+}$ cells in dermal papillae was 34.8 % (95 % CI: 28.8–40.9 %), and the proportion of *K5*$^{lin+}$ cells among SOX2-positive dermal papilla cells was 52.0 % (95 % CI: 42.0–62.1 %). The *K5*$^{lin+}$ fibroblasts were also maintained as DPCs and DSCs in the dorsal skin of aged mice (49 -weeks -old), suggesting a homeostatic function of the *K5*$^{lin+}$ hfDSCs to continually generate DPCs and DSCs throughout life (Fig. 2b).

### 2.3. *K5*$^{lin+}$ fibroblasts form the lower edge cells in dermal papilla at embryonic day 16.5

To investigate the emergence of *K5*$^{lin+}$ fibroblasts in developing hair follicles, we searched the fetal *Pα*-EGFP/*K5*$^{lin}$-tdTomato mouse skin for eGFP and tdTomato double-positive cells. On embryonic day 14.5 (E14.5), tdTomato fluorescence was expressed in the superficial layers of the skin and accumulated in the hair follicles of the whiskers (Fig. 3a). As hair follicles appeared throughout the body around E16.5, clusters of tdTomato-positive cells aligned with the developing hair follicles. Immunostaining of the dorsal skin at E14.5 showed that tdTomato fluorescence was fully detected in the epidermal monolayer (Fig. 3b). At E15.5, the fetal skin revealed clear formation of placodes and dermal condensates that consisted of the tdTomato-negative fibroblasts. At E16.5, *K5*$^{lin+}$ fibroblasts expressing relatively weak tdTomato fluorescence were detected at the lower edge of the primitive dermal papilla in elongating hair follicles, suggesting that fluctuating fibroblasts with a minor *Krt5* transcript are *K5*$^{lin+}$ cells. At E18.5, *K5*$^{lin+}$ fibroblasts were clearly identified in the dermal sheath cup where the hfDSCs had been shown to reside. Taken together with the scRNA-seq analysis, these observations suggest that *K5*$^{lin+}$ fibroblasts function as hfDSCs to form lower DPCs and DSCs during the development of hair follicles.

## 3. Discussion

In this study, we demonstrated the emergence of *K5*$^{lin+}$ fibroblasts in the fetal skin to develop hair follicle mesenchyme, which function as *Sox2*$^{+}$/*Acta2*$^{+}$ hfDSCs to generate lower DPCs and DSCs. The molecular and cellular mechanisms underlying the development of *K5*$^{lin+}$ hair follicle mesenchyme remain unknown. To elucidate the mechanism underlying the generation the *K5*$^{lin+}$ population in early DPCs at E16.5, it is necessary to determine whether they were generated through EMT from *Krt5*$^{+}$ keratinocytes or through genetic fluctuation to transiently open the *Krt5* chromatin locus in fibroblasts.

As *Krt5* is a marker of undifferentiated keratinocytes in the surface ectoderm, but not of mesodermal fibroblasts, *K5*$^{lin+}$ fibroblasts in the fetal skin seem to develop from ectodermal tissues. Immunohistochemical analysis of fetal skin indicated that the *K5*$^{lin+}$ fibroblasts appeared concurrently with hair follicle development in the upper dermis. Some dermal fibroblasts develop from neural crest cells, which are generated by the delamination of ectodermal epithelia in the neural fold and neural crest at E8.5, and E9.5, respectively [11,12]. Neural fold-derived neural crest cells develop from the non-neural surface ectoderm, which eventually forms an epidermis consisting of *Krt5*$^{+}$ epidermal keratinocytes. The non-neural surface ectoderm-derived neural crest cells then develop into ectodermal fibroblasts, which may be the origin of *K5*$^{lin+}$ fibroblasts in the fetal skin, to develop and maintain the hair follicle mesenchyme. Performing time-series scRNA-seq analyses of embryos for tracking the cell fate of *K5*$^{lin+}$ fibroblasts during fetal development might be helpful.

*K5*$^{lin+}$ fibroblasts in the hair follicle functioned as hfDSCs for generating lower DPCs and DSCs [13]. Shin et al. reported that DPCs consist of two distinct populations: upper (definitive) and lower (supplementary) DPCs [14]. Lower DPCs, as well as hfDSCs, have the potential to repair damaged DPCs, including upper DPCs, by reproducing new DPCs. Our results suggest that *K5*$^{lin+}$ fibroblasts are the major, if not exclusive, developmental origins of lower DPCs, however, the precise localization of *K5*$^{lin+}$ fibroblasts in dermal papillae should be

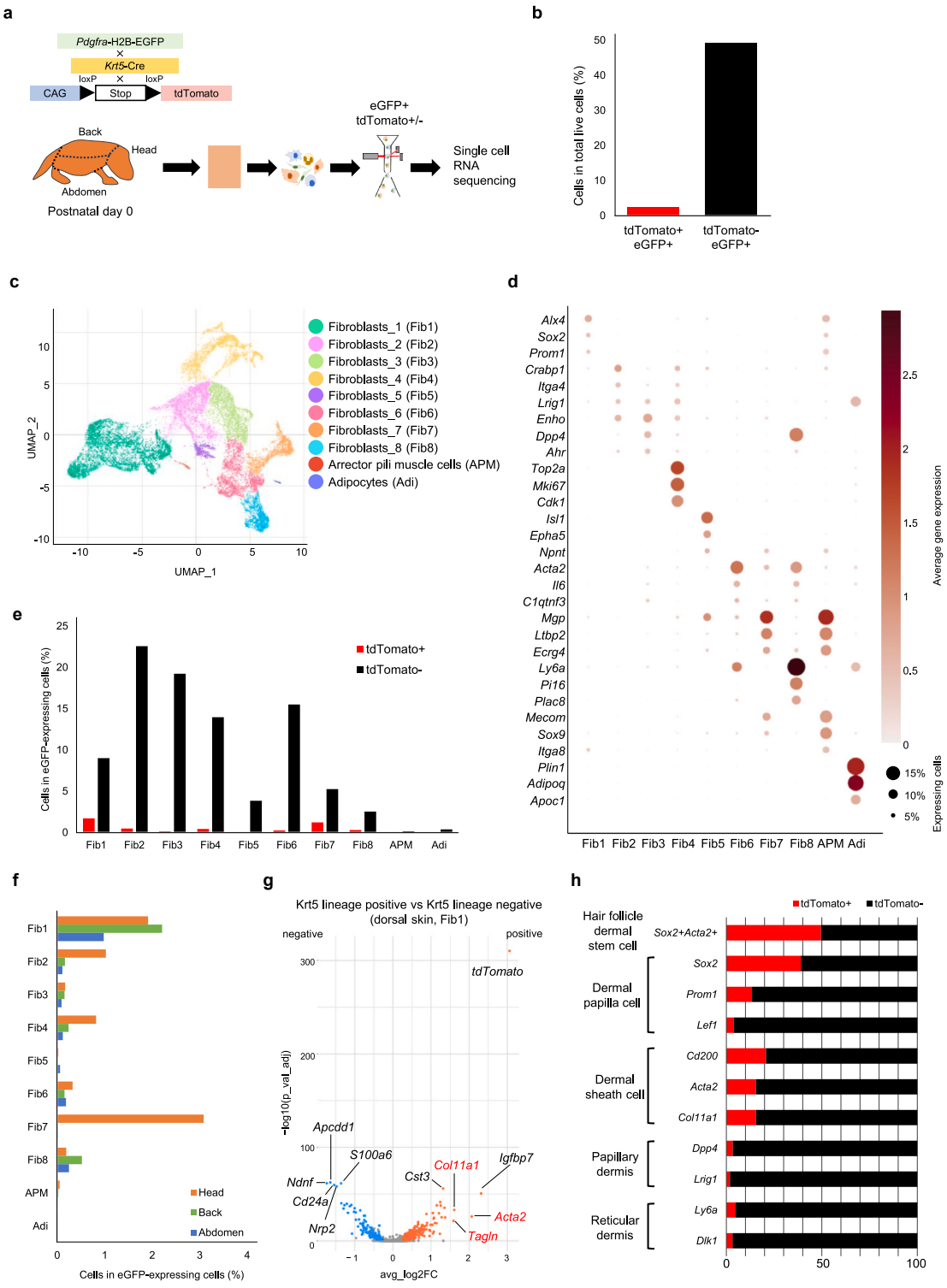


**Fig. 1.** Transcriptomic characters of $K5^{lin+}$ fibroblasts in the follicular mesenchyme

**a** The skin of the head, back, and abdomen from Pdgfra-H2B-EGFP; Krt5-Cre; ROSA-CAG-loxP-stop-loxP-tdTomato neonatal mice were harvested. The skin samples were dissociated into single cells, and eGFP+ and tdTomato± cells were sorted by FACS to perform single-cell RNA sequencing. Cells from three mice were pooled. **b** Quantitative analysis using flow cytometry presents the percentages of eGFP+ and tdTomato± cells in total live cells (2.45 % vs. 49.32 %). **c** Transcriptomes of fibroblasts were visualized with Uniform Manifold Approximation and Projection (UMAP) and colored according to 10 annotated clusters. **d** Bubble plots show the representative markers of clusters in (**c**). The circle color and size show average gene expression and percentage of expressing cells in each cluster, respectively. **e** Percentages of tdTomato± cells by cluster in eGFP+ cells are shown. Fib1(1.70 %) and Fib7 (1.23 %) account for relatively higher proportions than other clusters. **f** Percentages of tdTomato+ cells in eGFP+ cells are sorted by samples from the head, back, and abdomen. **g** The analysis of differentially expressed genes between tdTomato-positive and -negative fibroblasts in the Fib1 cluster shows that tdTomato+ cells dominantly expressed representative genes of dermal sheath cells, such as *Acta2*, *Col11a1*, and *Tagln*. **h** Proportion of tdTomato± cells expressing each representative gene for fibroblast subpopulations in dorsal skin fibroblasts are shown. The tdTomato+ cells shared approximately 50 % of the fibroblasts expressing both *Sox2*and *Acta2*.

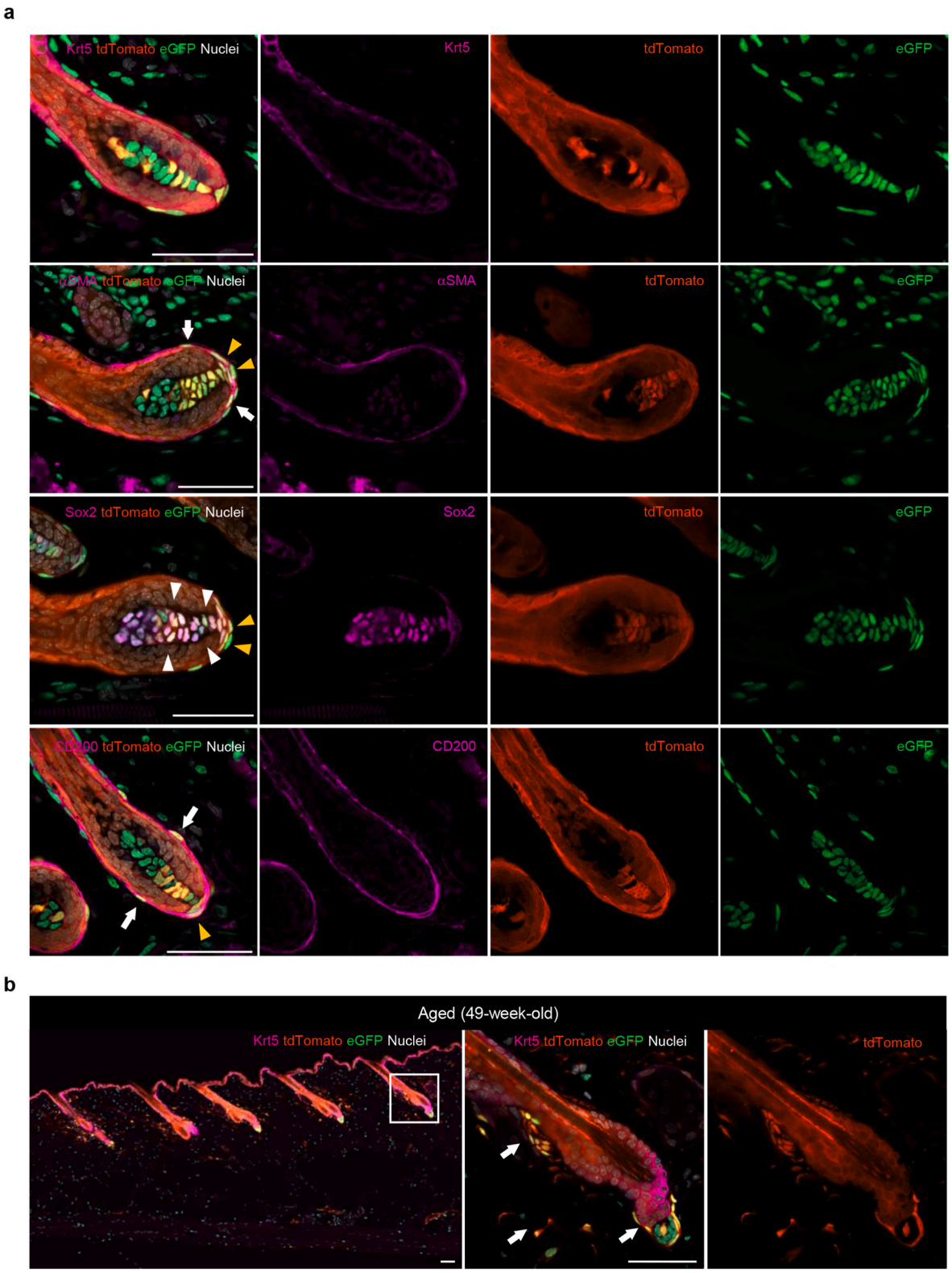


**Fig. 2.** Immunostaining of dorsal skin from Pdgfra-H2B-EGFP; Krt5-Cre; ROSA-CAG-loxP-stop-loxP-tdTomato neonatal and aged mice.
**a** Immunostaining of neonatal dorsal skin shows that both tdTomato- and eGFP- positive cells were observed in dermal papilla, expressing SOX2 (white arrowhead), and dermal sheath, expressing αSMA and CD200 (white arrow). Cells at dermal sheath cup, the edge of dermal papilla, were tdTomato-positive with expressing both SOX2 and αSMA (yellow arrowhead). Krt5 was not currently expressed in tdTomato- and eGFP- double positive cells. Scale bar = 50 μm **b** TdTomato expressing fibroblasts were located in dermal papilla, dermal sheath, and interstitial dermis (arrow) in aged (49-week-old) mice. Scale bar = 50 μm.

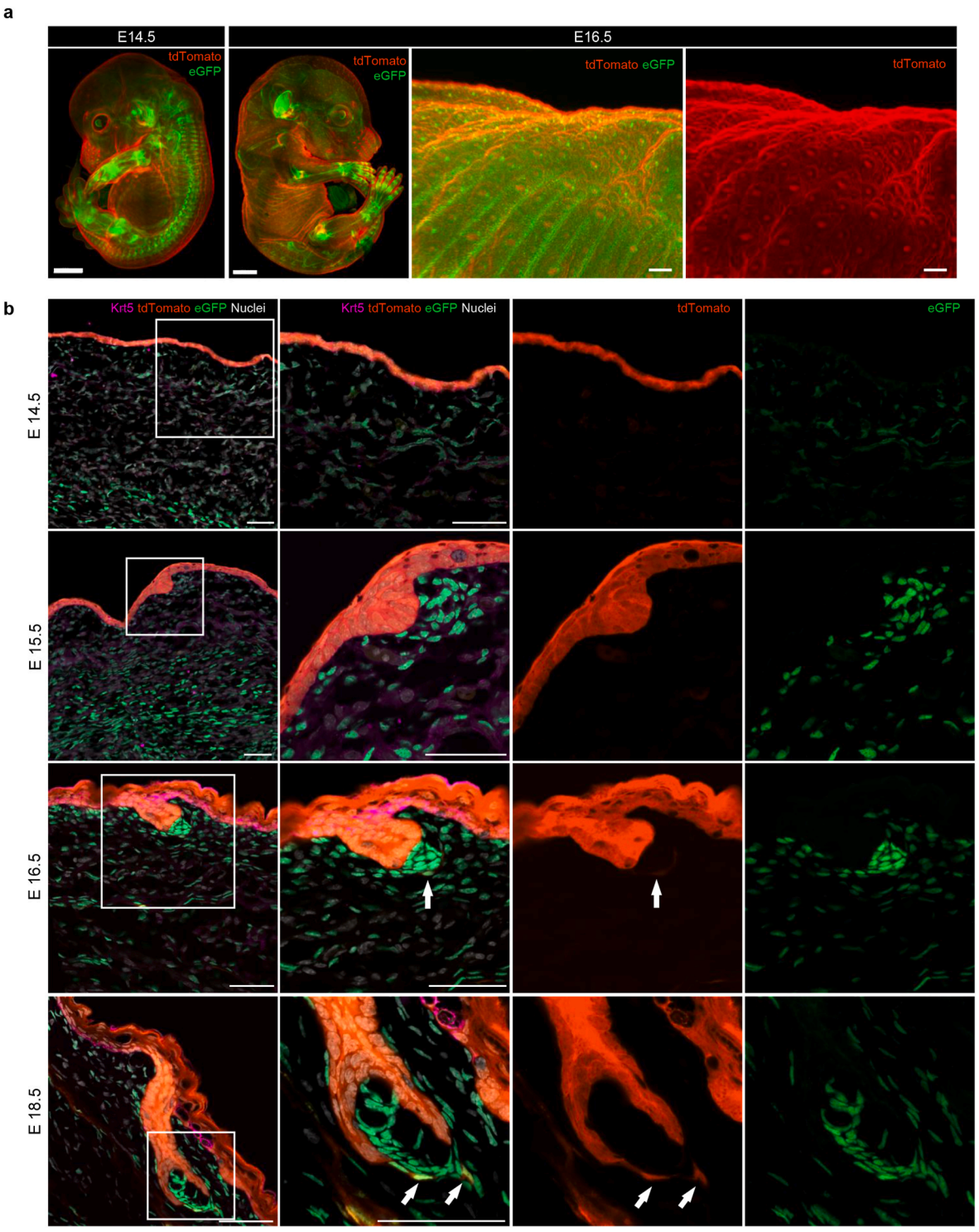


**Fig. 3.** Localization of tdTomato-positive fibroblasts in the hair follicle during fetal development.
**a** Images of whole mount embryo of Pdgfra-H2B-EGFP; Krt5-Cre; ROSA-CAG-loxP-stop-loxP-tdTomato mice at E14.5 and E16.5. Hair follicle structures were observed in the dorsal skin. Scale bar = 1500 μm. Expanded images of back are shown on the right. Scale bar = 200 μm **b** Time-series images of dorsal skin at E14.5, E15.5, E16.5, and E18.5. The eGFP-positive cells expressed tdTomato fluorescence weakly at E16.5 (arrow) and clearly at E18.5 in dermal sheath cup. Scale bar = 50 μm.

determined, for example by acquiring three-dimensional images. Predicting the differentiation pathway of $K5^{lin+}$ fibroblasts as the one of the origins of lower DPCs using trajectory analysis of scRNA-seq data should also be considered.

In terms of human DSCs, a previous report shows that DSCs are involved in de novo hair follicle formation [15]. Moreover, when DSCs from the occipital region were autologously transplanted to the head of patients with male/female pattern hair loss, hair density increased significantly [16]. In addition, human DSCs have the properties of mesenchymal stromal cells and promoted skin wound regeneration in diabetic model mice [17]. Therefore, the possibility that DSCs can be induced from epidermal cells is considerably advantageous in the regeneration of cutaneous wounds. In addition, whether DSC abnormalities are involved in human hair follicle diseases remains unclear,

and further research is needed to determine the association of DSCs, particularly the human counterpart of Krt5 lineage DSCs, with hair follicle malformations.

As the limitation of this study, we did not validate the functions of $K5^{lin+}$ fibroblasts in vivo and molecular mechanisms of EMT during hair morphogenesis. To estimate the function of $K5^{lin+}$ fibroblasts, we consider the transplantation of $K5^{lin+}$ fibroblasts from neonatal mice into other mice to observe the histological distribution. In addition, it is necessary to examine whether keratinocytes can be induced to differentiate into hfDSCs in vitro and in vivo under the condition of regulating EMT related transcription factors, such as *Snai1* and *Snai2* and signaling pathways which promote EMT process like TGF-β signaling pathway [18]. The alternative explanation of the appearance of $K5^{lin+}$ fibroblasts may be immature MET to develop DPCs, although the expression of *Snai1* and *Snai2* in DPCs supports EMT from epidermal cells.

To our knowledge, this is the first study to describe the presence of $K5^{lin+}$ fibroblasts in the skin and to highlight their function in the development and maintenance of the hair follicle mesenchyme. Our findings will provide a theoretical foundation for further research on the role and function of the $K5^{lin+}$ mesenchyme not only in cutaneous development, but also in cutaneous pathogenesis, and hopefully in cutaneous regeneration.

## 4. Materials and methods

### 4.1. Animals

B6.129S4-*Pdgfra*$^{tm11(EGFP)Sor}$/J (JAX stock 007669) [19], and B6.Cg-*Gt(ROSA)26Sor*$^{tm9(CAG-tdTomato)Hze}$/J (JAX stock 007909) [20] mice were purchased from Jackson Laboratory (Bar Harbor, ME, USA). Tg (KRT5-cre)1Tak mice were kindly provided by Junji Takeda of Osaka University, Osaka, Japan [21]. As nonspecific expression of Cre protein has been reported in female *Krt5*-cre transgenic mice, we crossed male *Krt5*-cre transgenic mice with female B6.129S4-*Pdgfra*$^{tm11(EGFP)Sor}$/J to obtain *Krt5*-cre; B6.129S4-*Pdgfra*$^{tm11(EGFP)Sor}$/J male mice. Then, *Krt5*-cre; B6.129S4-*Pdgfra*$^{tm11(EGFP)Sor}$/J male mice were crossed with ROSA-CAG-loxP-stop-loxP-tdTomato female mice and confirmed no ubiquitous expression of tdTomato fluorescence [22]. All animals were housed in a specific pathogen-free environment under a normal light-dark cycle (12/12 h). All mice were handled in accordance with the guidelines approved by the Animal Committee of the Osaka University Graduate School of Medicine (approval number 04-065-009, Approval Date:20240213). The study was conducted following the ARRIVE guidelines.

### 4.2. Cell isolation

The *Pdgfra*-H2B-EGFP; *Krt5*-Cre; ROSA-CAG-loxP-stop-loxP-tdTomato neonatal mice were euthanized by decapitation after anesthesia with isoflurane (Viatris, Canonsburg, PA, USA), and full-thickness skins from the head, back and abdomen were excised. The collected skin was minced using scissors. Tissue pieces were dissociated enzymatically in 3 mL of RPMI (Nacalai Tesque, Kyoto, Japan) containing 5 % fetal bovine serum (FBS; Thermo Fisher Scientific, Waltham, MA, USA) and 0.3 % Liberase™ (Merck, Darmstadt, Germany) at 37 °C for 30 min. Subsequently, the obtained cell suspensions were collected and the remaining tissues that were not dissociated were treated with RPMI containing Liberase once again. Then, the residual tissues were treated with 2 mL of TrypLE™ Select Enzyme (Thermo Fisher Scientific) at 37 °C for 15 min. The obtained cell suspensions were filtered through a 70-μm cell strainer and washed in minimum essential medium alpha (Thermo Fisher Scientific) with 2 % FBS. Samples from three mice were pooled and cell suspensions from the head, back, and abdomen were obtained.

### 4.3. Single-cell RNA sequencing

Isolated cells from the head, back, and abdomen were individually labelled using the 3′ CellPlex Kit Set A (10x Genomics, Pleasanton, CA, USA). Labelling was performed according to the CG000391 "Cell Multiplexing Oligo Labelling for Single Cell RNA Sequencing Protocol" from 10x Genomics. SYTOX Blue dead cell stain (Thermo Fisher Scientific) was added to the labelled cell suspension. SYTOX-negative, eGFP-positive, and tdTomato-positive or -negative cells were sorted using the BD FACS Aria III system (BD Biosciences, Franklin Lakes, NJ, USA). The gating strategies are detailed in Supplementary Fig. 1. The sorted cells were washed with phosphate-buffered saline (PBS) containing 0.04 % bovine serum albumin and resuspended. Libraries were prepared according to the CG000388 "Chromium Next GEM Single Cell 3' Reagent Kits v3.1 (Dual Index) with Feature Barcode technology for Cell Multiplexing" protocol from 10x Genomics. The prepared libraries were sequenced using a NovaSeq 6000 platform (Illumina, San Diego, CA, USA).

### 4.4. Bioinformatics

Sequencing outputs were demultiplexed using CellRanger mkfastq [23] with default options. The demultiplexed fastq files were aligned to the mouse reference genome (mm10), and counts were conducted using Cell Ranger Multi with the default options. Data analysis was performed using the R package Seurat (version 5.0.3) [24]. CellRanger outputs were filtered using the number of transcripts and genes and the percentages of mitochondrial genes. Data in each cell were normalized using the LogNormalize method, and principal component analysis was performed to visualize single-cell clustering by Uniform Manifold Approximation and Projection (UMAP). The sub-cluster which expressed representative fibroblast marker genes (*Pdgfra*, *Col1a1*, *Vim*, and *Dpt*) was extracted to focus on the transcriptomic analysis of the fibroblast population. The cell clusters were determined using the FindClusters function, and similar clusters were grouped manually. Differential gene expression analysis was performed using Seurat with the test.use = 'MAST' option.

### 4.5. Histology and immunohistochemistry

The collected skin tissues were soaked in 4 % paraformaldehyde for 12–18 h followed by 30 % sucrose in phosphate-buffered saline (PBS), embedded in Tissue-Tec OCT compound (Sakura Finetek Japan, Tokyo, Japan), and frozen at −20 °C. Frozen tissues were sectioned at 8 or 14 μm thickness. The samples were blocked with 3 % bovine serum albumin (BSA), 0.3 % TritonTMX-100 (Merck), and 0.3 % Polyoxyethylene Sorbitan Monolaurate (Nacalai Tesque) in PBS at 20–25 °C for 1 h. Then, the sections were incubated with rabbit polyclonal anti-mouse keratin 5 (905503, 1:500; BioLegend, San Diego, CA, USA), goat monoclonal anti-mouse SOX2 (AF2018, 5 μg/mL; R&D Systems, Minneapolis, MN, USA), and rabbit monoclonal anti-mouse smooth muscle actin (ab5694, 1:100; Abcam, Cambridge, UK) at 20–25 °C for 18 h. The sections were washed with PBS three times and incubated with Hoechest33342 (1:500; Thermo Fisher Scientific) and Alexa Fluor 647-conjugated goat anti-rabbit IgG (A21245, 1:200; Thermo Fisher Scientific) or Alexa Fluor 647-conjugated donkey anti-goat IgG (A21447, 1:200; Thermo Fisher Scientific) secondary antibodies at 20–25 °C for 4 h. The samples were washed with PBS three times and mounted in ProLong Gold antifade mountant (Thermo Fisher Scientific). The skin sections were observed using an Airyscan confocal laser-scanning microscope (LSM980; Carl Zeiss, Oberkochen, Germany).

### 4.6. Animal tissue clearing

The whole body of embryo at E14.5 and E16.5 were fixed with 4 % paraformaldehyde at 20–25 °C for 6 h, and then tissue clearing was

conducted using CUBIC-L (Tokyo Chemical Industry, Tokyo, Japan) and CUBIC-R+(M) (Tokyo Chemical Industry) reagents as previously described [25,26]. First, fixed samples were immersed in 50 % CUBIC-L diluted with distilled water at 20–25 °C for 24 h followed by in 100 % CUBIC-L for 24 h. Subsequently, the specimens were washed with PBS for three times and immersed in 50 % CUBIC-R+(M) diluted with distilled water at 20–25 °C for 24 h, then in 100 % CUBIC-R+(M) for 24 h. Finally, the samples were set on the glass bottom dish (MATSUNAMI GLASS, Osaka, Japan) immersed in 100 % CUBIC-R+(M). Images were acquired using a Ti2-E confocal microscope (Nikon, Tokyo, Japan).

### 4.7. Statistics

We did not apply a specific statistical method to determine the sample size. No blinding or randomization was used for data analysis.

## CRediT authorship contribution statement

**Yoshikazu Hirose:** Writing – original draft, Investigation, Formal analysis, Data curation. **Asaka Miura:** Investigation, Formal analysis, Data curation. **Yuya Ouchi:** Writing – original draft, Software, Formal analysis. **Tomomi Kitayama:** Writing – original draft, Investigation, Data curation. **Souki Omura:** Data curation. **Takashi Shimbo:** Supervision. **Akio Tanaka:** Supervision. **Manabu Fujimoto:** Supervision. **Kotaro Saga:** Supervision. **Katsuto Tamai:** Writing – review & editing, Project administration, Funding acquisition, Conceptualization.

## Data availability

The single-cell RNA sequencing data are available within the article. These data were deposited in the GEO database under the accession code GSE280868.

## Funding sources

This study was supported by JSPS KAKENHI [grant number JP19H03682] and academia-industry collaboration grant by StemRIM.

## Declaration of competing interest

Katsuto Tamai is a scientific founder of and received research funding from StemRIM.

Katsuto Tamai and Takashi Shimbo are StemRIM stockholders.

Yuya Ouchi and Tomomi Kitayama are employees of StemRIM.

The other authors declare no competing interests.

## Acknowledgements

We thank Sho Yamazaki, Machika Kawamura, Atsuki Shimizu and Yoshiki Okita of StemRIM, Inc. for their technical support. We would like to thank the Nikon Imaging Center at Osaka University for technical support.

## Appendix A. Supplementary data

Supplementary data to this article can be found online at https://doi.org/10.1016/j.bbrep.2025.102006.

## References

[1] H.E. Talbott, S. Mascharak, M. Griffin, D.C. Wan, M.T. Longaker, Wound healing, fibroblast heterogeneity, and fibrosis, Cell Stem Cell 29 (2022) 1161–1180, https://doi.org/10.1016/j.stem.2022.07.006.

[2] R.R. Driskell, F.M. Watt, Understanding fibroblast heterogeneity in the skin, Trends Cell Biol. 25 (2015) 92–99, https://doi.org/10.1016/j.tcb.2014.10.001.

[3] M. Sieber-Blum, M. Grim, The adult hair follicle: cradle for pluripotent neural crest stem cells, Birth Defects Res. C Embryo Today 72 (2004) 162–172, https://doi.org/10.1002/bdrc.20008.

[4] J.H.P. Dawes, R.N. Kelsh, Cell fate decisions in the neural crest, from pigment cell to neural development, Int. J. Mol. Sci. 22 (2021) 13531, https://doi.org/10.3390/ijms222413531.

[5] K.J. Fernandes, I.A. McKenzie, P. Mill, K.M. Smith, M. Akhavan, F. Barnabé-Heider, J. Biernaskie, A. Junek, N.R. Kobayashi, J.G. Toma, D.R. Kaplan, P.A. Labosky, V. Rafuse, C.C. Hui, F.D. Miller, A dermal niche for multipotent adult skin-derived precursor cells, Nat. Cell Biol. 6 (2004) 1082–1093, https://doi.org/10.1038/ncb1181.

[6] A.E. Parent, K.M. Newkirk, D.F. Kusewitt, Slug (Snai2) expression during skin and hair follicle development, J. Invest. Dermatol. 130 (2010) 1737–1739, https://doi.org/10.1038/jid.2010.22.

[7] C. Jamora, P. Lee, P. Kocieniewski, M. Azhar, R. Hosokawa, Y. Chai, E. Fuchs, A signaling pathway involving TGF-beta2 and snail in hair follicle morphogenesis, PLoS Biol. 3 (2005) e11, https://doi.org/10.1371/journal.pbio.0030011.

[8] M. Rendl, L. Polak, E. Fuchs, BMP signaling in dermal papilla cells is required for their hair follicle-inductive properties, Genes Dev. 22 (2008) 543–557. http://www.genesdev.org/cgi/doi/10.1101/gad.1614408.

[9] N. Oshimori, E. Fuchs, Paracrine TGF-β signaling counterbalances BMP-mediated repression in hair follicle stem cell activation, Cell Stem Cell 10 (2012) 63–75, https://doi.org/10.1016/j.stem.2011.11.005.

[10] A. Hagner, W. Shin, S. Sinha, W. Alpaugh, M. Workentine, S. Abbasi, W. Rahmani, N. Agabalyan, N. Sharma, H. Sparks, J. Yoon, E. Labit, J. Cobb, I. Dobrinski, J. Biernaskie, Transcriptional profiling of the adult hair follicle mesenchyme reveals R-spondin as a novel regulator of dermal progenitor function, iScience 23 (2020) 101019, https://doi.org/10.1016/j.isci.2020.101019.

[11] M.A. Breau, T. Pietri, M.P. Stemmler, J.P. Thiery, J.A. Weston, A nonneural epithelial domain of embryonic cranial neural folds gives rise to ectomesenchyme, Proc. Natl. Acad. Sci. U. S. A 105 (2008) 7750–7755, https://doi.org/10.1073/pnas.0711344105.

[12] R.A. Keuls, Y.S. Oh, I. Patel, R.J. Parchem, Post-transcriptional regulation in cranial neural crest cells expands developmental potential, Proc. Natl. Acad. Sci. U. S. A 120 (2023) e2212578120, https://doi.org/10.1073/pnas.2212578120.

[13] W. Rahmani, S. Abbasi, A. Hagner, E. Raharjo, R. Kumar, A. Hotta, S. Magness, D. Metzger, J. Biernaskie, Hair follicle dermal stem cells regenerate the dermal sheath, repopulate the dermal papilla, and modulate hair type, Dev. Cell 31 (2014) 543–558, https://doi.org/10.1016/j.devcel.2014.10.022.

[14] W. Shin, N.L. Rosin, H. Sparks, S. Sinha, W. Rahmani, N. Sharma, M. Workentine, S. Abbasi, E. Labit, J.A. Stratton, J. Biernaskie, Dysfunction of hair follicle mesenchymal progenitors contributes to age-associated hair loss, Dev. Cell 53 (2020) 185–198, https://doi.org/10.1016/j.devcel.2020.03.019, e7.

[15] A.J. Reynolds, C. Lawrence, P.B. Cserhalmi-Friedman, A.M. Christiano, C. A. Jahoda, Trans-gender induction of hair follicles, Nature 402 (1999) 33–34, https://doi.org/10.1038/46938.

[16] R. Tsuboi, S. Niiyama, R. Irisawa, K. Harada, Y. Nakazawa, J. Kishimoto, Autologous cell-based therapy for male and female pattern hair loss using dermal sheath cup cells: a randomized placebo-controlled double-blinded dose-finding clinical study, J. Am. Acad. Dermatol. 83 (2020) 109–116, https://doi.org/10.1016/j.jaad.2020.02.033.

[17] D. Ma, J.E. Kua, W.K. Lim, S.T. Lee, A.W. Chua, In vitro characterization of human hair follicle dermal sheath mesenchymal stromal cells and their potential in enhancing diabetic wound healing, Cytotherapy 17 (2015) 1036–1051, https://doi.org/10.1016/j.jcyt.2015.04.001.

[18] J. Xu, S. Lamouille, R. Derynck, TGF-beta-induced epithelial to mesenchymal transition, Cell Res. 19 (2009) 156–172, https://doi.org/10.1038/cr.2009.5.

[19] T.G. Hamilton, R.A. Klinghoffer, P.D. Corrin, P. Soriano, Evolutionary divergence of platelet-derived growth factor alpha receptor signaling mechanisms, Mol. Cell Biol. 23 (2003) 4013–4025, https://doi.org/10.1128/MCB.23.11.4013-4025.2003.

[20] L. Madisen, T.A. Zwingman, S.M. Sunkin, S.W. Oh, H.A. Zariwala, H. Gu, L.L. Ng, R.D. Palmiter, M.J. Hawrylycz, A.R. Jones, E.S. Lein, H. Zeng, A robust and high-throughput Cre reporting and characterization system for the whole mouse brain, Nat. Neurosci. 13 (2010) 133–140, https://doi.org/10.1038/nn.2467.

[21] M. Tarutani, S. Itami, M. Okabe, M. Ikawa, T. Tezuka, K. Yoshikawa, T. Kinoshita, J. Takeda, Tissue-specific knockout of the mouse Pig-a gene reveals important roles for GPI-anchored proteins in skin development, Proc. Natl. Acad. Sci. U. S. A 94 (1997) 7400–7405, https://doi.org/10.1073/pnas.94.14.7400.

[22] A. Ramirez, A. Page, A. Gandarillas, J. Zanet, S. Pibre, M. Vidal, L. Tusell, A. Genesca, D.A. Whitaker, D.W. Melton, J.L. Jorcano, A keratin K5Cre transgenic line appropriate for tissue-specific or generalized Cre-mediated recombination, Genesis 39 (2004) 52–57, https://doi.org/10.1002/gene.20025.

[23] G.X.Y. Zheng, J.M. Terry, P. Belgrader, P. Ryvkin, Z.W. Bent, R. Wilson, S. B. Ziraldo, T.D. Wheeler, G.P. McDermott, J. Zhu, M.T. Gregory, J. Shuga, L. Montesclaros, J.G. Underwood, D.A. Masquelier, S.Y. Nishimura, M. Schnall-Levin, P.W. Wyatt, C.M. Hindson, R. Bharadwaj, A. Wong, K.D. Ness, L.W. Beppu, H.J. Deeg, C. McFarland, K.R. Loeb, W.J. Valente, N.G. Ericson, E.A. Stevens, J. P. Radich, T.S. Mikkelsen, B.J. Hindson, J.H. Bielas, Massively parallel digital transcriptional profiling of single cells, Nat. Commun. 8 (2017) 14049, https://doi.org/10.1038/ncomms14049.

[24] A. Butler, P. Hoffman, P. Smibert, E. Papalexi, R. Satija, Integrating single-cell transcriptomic data across different conditions, technologies, and species, Nat. Biotechnol. 36 (2018) 411–420, https://doi.org/10.1038/nbt.4096.
[25] E.A. Susaki, K. Tainaka, D. Perrin, F. Kishino, T. Tawara, T.M. Watanabe, C. Yokoyama, H. Onoe, M. Eguchi, S. Yamaguchi, T. Abe, H. Kiyonari, Y. Shimizu, A. Miyawaki, H. Yokota, H.R. Ueda, Whole-brain imaging with single-cell resolution using chemical cocktails and computational analysis, Cell 157 (2014) 726–739, https://doi.org/10.1016/j.cell.2014.03.042.
[26] K. Matsumoto, T.T. Mitani, S.A. Horiguchi, J. Kaneshiro, T.C. Murakami, T. Mano, H. Fujishima, A. Konno, T.M. Watanabe, H. Hirai, H.R. Ueda, Advanced CUBIC tissue clearing for whole-organ cell profiling, Nat. Protoc. 14 (2019) 3506–3537, https://doi.org/10.1038/s41596-019-0240-9.